Optimizing slow and stored light for multidisciplinary applications

Mason Klein[a,b], Yanhong Xiao[a], Alexey V. Gorshkov[b], Michael Hohensee[a,b], Cleo D. Leung[a,b], Mark R. Browning[a,b], David F. Phillips[a], Irina Novikova[c], Ronald L. Walsworth[a,b]

[a]Harvard-Smithsonian Center for Astrophysics, Cambridge, MA, 02138 USA
[b]Department of Physics, Harvard University, Cambridge, MA, 02138 USA
[c]Department of Physics, College of William & Mary, Williamsburg, VA 23185, USA

December 24, 2007

ABSTRACT

We present a preliminary experimental study of the dependence on optical depth of slow and stored light pulses in Rb vapor. In particular, we characterize the efficiency of slow and stored light as a function of Rb density; pulse duration, delay and storage time; and control field intensity. Experimental results are in good qualitative agreement with theoretical calculations based on a simplified three-level model at moderate densities.

Keywords: Electromagnetically-induced transparency, slow light, stored light, vapor cell, buffer gas, optical depth

1. INTRODUCTION

Applications of slow and stored light based on electromagnetically-induced transparency (EIT), in both quantum information processing and optical communication, will benefit from improved efficiency and delay-bandwidth product. In quantum information, stored light has emerged as a promising technique for applications such as single-photon generation on demand[1–5] and quantum memories[6–8] and repeaters.[9–11] However, practical applications will require significant improvements in the efficiency of writing, storing, and retrieving an input photon state beyond values achieved to date.[12–15] In classical communications, optical buffers require adjustable delay time (i.e., group index) for input signal pulses with minimal pulse distortion and loss[16] and high compression of the input pulse for high data density inside the delay medium. However, high efficiency and large delay-bandwidth product have not fully been realized in all-optical systems. Here we present a preliminary study of the optimization of slow and stored light using EIT in warm Rb vapor as a function of optical depth, laser power, and input pulse bandwidth.

In EIT, a weak signal pulse propagates with very slow group velocity through an otherwise absorbing medium,[17] which is established by a strong control field. The reduced group velocity with which a signal propagates under EIT is the result of the transfer of photonic excitation in the pulse to the collective spin coherence of the atoms. The group velocity is proportional to the control field intensity, and can be reduced to zero by shutting off the control light. In this case the photonic information of the pulse is completely transferred to the atoms. This coherent transfer is reversible, and thus after some storage time the pulse may be retrieved, converting it back into photonic excitation when the control light is turned back on.

Optimization of slow and stored light requires reducing the absorption of signal light and spin decoherence, as well as increasing optical depth to achieve large delay-bandwidth product.[18] In warm atom vapor cells, signal light absorption is typically driven by incomplete polarization of the atomic medium due to such mechanisms as radiation trapping and competing nonlinear processes. Atomic decoherence arises from mechanisms such as collisions with buffer gas atoms and cell walls, diffusion out of the laser beam, and residual magnetic field gradients.

Advances in Slow and Fast Light, edited by Selim M. Shahriar, Philip R. Hemmer, John R. Lowell,
Proc. of SPIE Vol. 6904, 69040C, (2008) · 0277-786X/08/$18 · doi: 10.1117/12.772216

Modeling the atomic medium as a collection of stationary three-level Λ-systems (Fig. 1a), we find that slow and stored light properties improve with increasing rubidium density or optical depth. The EIT bandwidth, γ_{EIT}, for moderate to large optical depths is found to be[19, 20]

$$\gamma_{EIT} = \frac{|\Omega_C|^2}{\sqrt{\gamma g^2 N L/c}} \tag{1}$$

where Ω_C is the Rabi frequency of the control field, γ the excited-state line width, N the total number of three-level atoms, L the length of the medium (the optical depth, $d = g^2 N L/\gamma c$), g the light-atom coupling coefficient, and c the speed of light. Similarly, the group velocity v_g resulting from the steep resonant dispersion for the signal pulse in the slow light medium is[19, 20]

$$v_g = \frac{c}{1 + g^2 N/|\Omega_C|^2} \approx \frac{c|\Omega_C|^2}{g^2 N}. \tag{2}$$

The absolute pulse delay, $\Delta T_{\rm abs}$, is then given by the length of the medium divided by the group velocity and we find that $\Delta T_{\rm abs} \propto d$, that is the delay is proportional to the optical depth. A careful theoretical study of storage efficiency η (defined as the ratio of the number of output photons to the number of input photons), optimized for a given optical depth,[21] finds that the optimal temporal pulse width $T_{opt} \sim d$, and that η scales as $1 - 19/d$ at high optical depth, and increases more rapidly at lower d. This treatment implies continued efficiency improvement with increasing optical depth. In practice, experiments have found that slow and stored light efficiency improves with increasing optical depth for modest optical depths. However, at larger optical depths, slow and stored light efficiency reach a maximum and then degrade. Note that a procedure for optimizing stored light efficiency for a given d, using the time-reversed output pulse to determine the shape of the input pulse, has been developed theoretically[21] and directly implemented experimentally.[22]

In the present study we report preliminary experimental investigations of the behavior of slow and stored light over a wide range of optical depths, by varying the temperature of Rb in a vapor cell. Measuring coherence loss rates and including them in the efficiency optimization model yields good agreement between theory and experiment as η falls off with increasing atomic density. We focus on the role played by optical depth in coherence loss, in particular the effect of radiation trapping, where incoherent photons are repeatedly re-absorbed by the medium before exiting.[23] We also report promising preliminary efficiency results for a new cell geometry designed to reduce coherence loss due to radiation trapping.

2. EXPERIMENTAL SETUP

We measured EIT and slow and stored light, using the D_1 transition in a warm ^{87}Rb vapor. The relevant energy levels and coupling fields are shown in Fig. 1a: a strong control field is resonant with $F = 2 \rightarrow F' = 2$ transition and a weak signal field is resonant with the $F = 1 \rightarrow F' = 2$. The optical fields were generated by an external cavity diode laser tuned to $\lambda = 795$ nm, amplified by a tapered amplifier, and spatially filtered by a pinhole (Fig. 1b). An electro-optic modulator (EOM) phase modulated the laser at the ground state hyperfine splitting (~ 6.835 GHz); the $+1$ sideband acted as the signal field, with a maximum signal to control intensity ratio of 2.5%; the sideband amplitude was varied to shape the desired signal pulse. The frequency could be varied to change the two-photon detuning δ of the EIT transition for measuring its line shape. The overall intensity was regulated with an acousto-optic modulator (AOM), which also shifted the frequency by +80 MHz. A quarter-wave plate ($\lambda/4$) before the cell converted the beam to circular polarization. The collimated beam entering the cell had a diameter of approximately 7 mm. The output fields were measured by sending the laser into an optical fiber, then into a fast photodetector (PD) along with a reference beam picked off prior to the EOM and AOM. The control field, signal field, or the unused -1 sideband could thus be measured by beat note detection with a spectrum analyzer, at 80 MHz, 6.835 GHz +80 MHz, and 6.835 GHz $-$ 80 MHz respectively. The transmission of the -1 sideband (off EIT resonance), being ~ 6 GHz away from any Rb resonance, was used as a reference for determining slow light delay or storage efficiency, where ΔT_{abs} was the difference between pulse peak times and efficiency $\eta =$ (signal pulse area)/(-1 sideband area).

The cell was housed in a plastic oven, which was heated by blown warm air. The cell temperature was varied between 39 and 79 °C, or atomic number density between 3.8×10^{10} and 1.1×10^{12} cm^{-3}. Three layers of

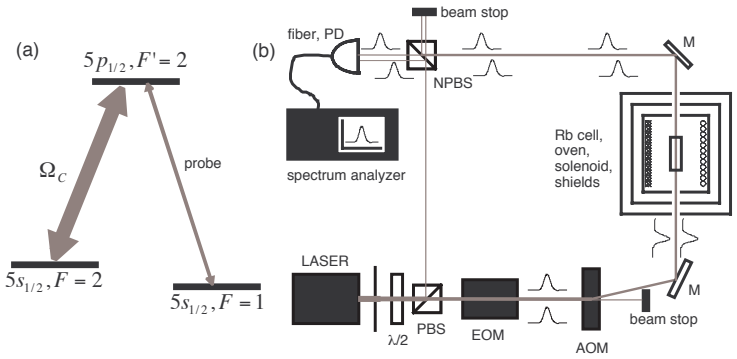

Figure 1. (a) The relevant ^{87}Rb atomic energy levels in a Λ-scheme used for EIT, slow, and stored light measurements. (b) Schematic of the apparatus. Output of laser is split with a half-wave plate ($\lambda/2$) and polarizing beam splitter (PBS) into a reference beam and main beam; electro-optic (EOM) and acousto-optic (AOM) modulators shape the signal and control fields; the vapor cell is housed inside an oven, solenoid, and magnetic shielding; a fast photodetector measures the beat between the unmodulated reference beam and the output from the vapor cell. *See text for details.*

cylindrical high-permeability shielding surrounded the oven to screen out stray laboratory magnetic fields, and a solenoid inside was used to cancel any small constant background field. Three Rb vapor cells were used in our experiments; all three contained isotopically enriched ^{87}Rb and were filled with buffer gas to confine atoms and extend their coherence life times. The cell used for all measurements except where specifically noted had length $L = 7.5$ cm and diameter $D = 2.5$ cm, and was filled with 40 Torr of Ne.

3. SLOW AND STORED LIGHT EFFICIENCY MEASUREMENTS

We studied slow and stored light as a function of optical depth by measuring the delay-bandwidth product and efficiency of "optimized" pulses as the vapor cell temperature was varied. Such pulses were constructed through an iterative optimization procedure in which a signal pulse was stored and retrieved, its output shape measured and a new pulse stored with the shape of the output pulse. This process is repeated until convergence. This procedure has been shown both theoretically[21] and experimentally[22] to produce slow-light pulse shapes that optimize storage efficiency for the given optical depth and laser power. In effect this procedure selects a pulse bandwidth balancing fractional delay and absorption to yield the largest output signal pulse.

Measured EIT bandwidths and slow light delays scaled as expected with optical depth. Figure 2a shows EIT linewidth (FWHM, as extracted from a Lorentzian fit) vs. atomic density, which follows the $\gamma_{EIT} \propto 1/\sqrt{d}$ trending expected from Eq. 1. Figure 2b shows that absolute pulse delay $\Delta T_{abs} \propto d$; and Figure 2c shows that the optimal pulse width $T_{opt} \propto d$. We measured line widths and delays at two control field powers, 3.8 mW and 8.8 mW, corresponding to respective intensities of 10 and 23 mW/cm^2 and Rabi frequencies of 6.7 and 10 MHz. Slow light delays in Figs. 2b and 2c are tailored for optimized stored light, obtaining neither the maximum absolute delay (achieved for a temporally long pulse experiencing only the steepest part of the dispersion but having a small fraction of the pulse in the atomic medium at one time) nor the maximum fractional delay (achieved for a short pulse which suffers large absorption due to frequency components outside the EIT bandwidth). Comparing the optimized pulse bandwidth (where T_{opt} is the temporal pulse width) to the measured EIT bandwidth (Fig. 2d), we find that $1/T \sim \gamma_{EIT}/3$, over a large range of fractional delays (from 0.2 to > 1.0), a somewhat greater pulse bandwidth than expected theoretically,[20,24] where $\gamma_{EIT}T >> 1$ or even $>> 10$. Note that based on the scalings of $\Delta T_{abs} \sim d$ and $T_{opt} \sim d$, we would expect the optimal frequency bandwidth to be quadratic in the EIT line width which is not clearly observed in Fig. 2d.

Stored light efficiency was measured for a range of rubidium densities between 4×10^{10} cm^{-3} (40 °C) and 1×10^{12} cm^{-3} (80 °C) and storage intervals from $\tau = 50$ μs to $\tau = 1.5$ ms and plotted for $\tau = 400$ μs in Fig. 3. The efficiencies peak at temperatures between 60 and 65 °C, falling at higher optical depth. The $1/e$ coherence lifetime during storage (Fig. 4) also fall at high density. This points to possible high-density

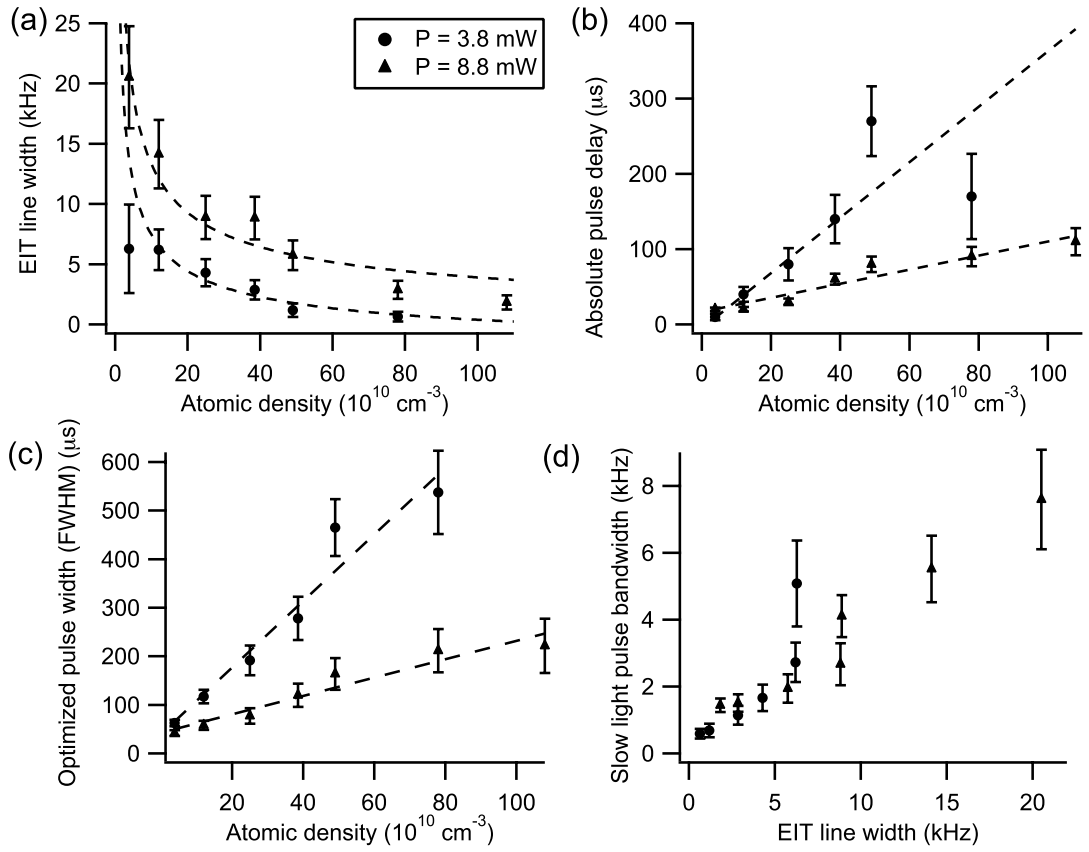

Figure 2. Measured EIT line width, slow light delay, and optimized pulse width at various optical depths and for two control field powers (3.8 mW and 8.8 mW). (a) EIT line widths are consistent with power broadening and density narrowing. (b) Absolute pulse delay (= time elapsed between the peaks of the reference pulse and the slowed pulse) and (c) optimized temporal pulse width are approximately linear in atomic density. (d) Optimized slow light bandwidth vs. EIT line width. Error bars for all measurements are derived from a systematic uncertainty in the Rb temperature of ~ 2 °C and uncertainty in the laser frequency of ~ 150 MHz. Dashed lines are fits of data to the simplified three-level model described in text.

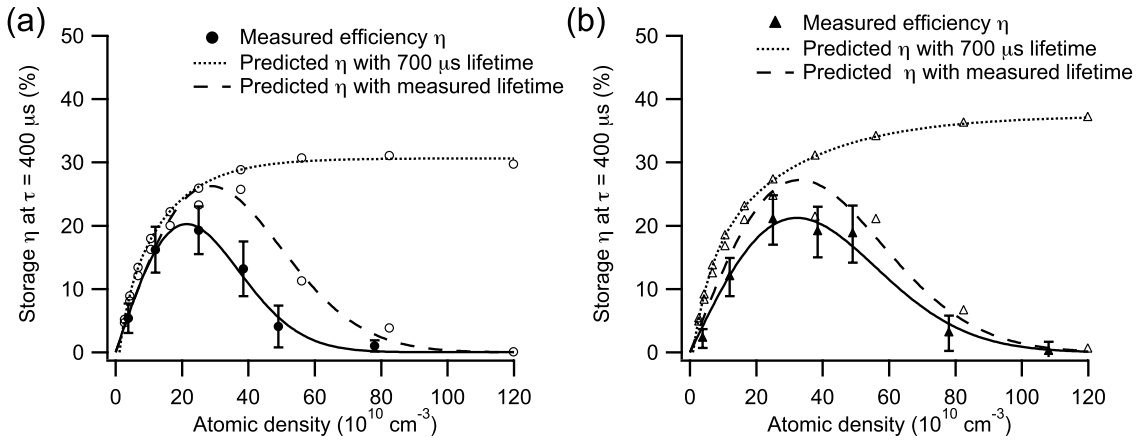

Figure 3. Measured and calculated storage efficiency at fixed storage time $\tau = 400$ μs vs. atomic density for control field laser powers of (a) 3.8 mW and (b) 8.8 mW. Theoretical predictions are shown both for a coherence lifetime of 700 μs with no density-dependent decoherence (dotted curves) and for the measured coherence lifetimes shown in Fig. 4 (dashed curves). Comparison of the two calculated results shows that density or temperature-dependent decoherence during the storage interval dominates high-density losses. The remaining discrepancy between measurement and calculation is likely due to radiation trapping. Error bars are from systematic uncertainty in Rb temperature of ~ 2 °C and of the laser frequency of ~ 150 MHz. *Curves added to guide the eye.*

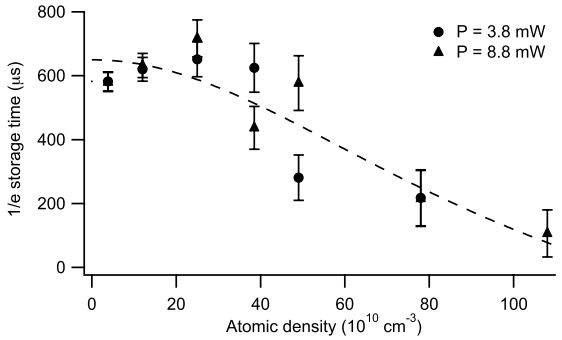

Figure 4. Lifetimes of stored coherence as a function of atomic density, derived from measurements described in text. The coherence lifetime drops at high atomic density, likely due to the effect of temperature-dependent losses such as Rb-Rb spin exchange. Error bars are derived from Rb temperature and laser frequency uncertainty as well as statistical uncertainty in fits to coherence lifetimes. *Dashed line added to guide the eye.*

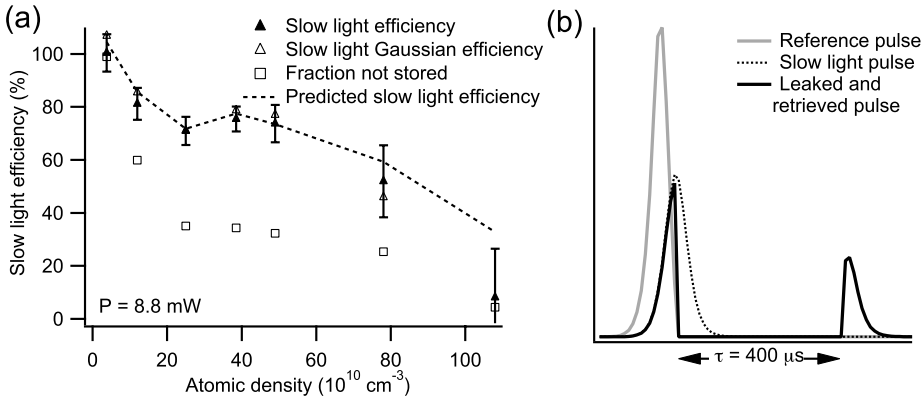

Figure 5. (a) Slow light efficiency (output pulse area divided by input pulse area) as a function of atomic density, for input pulse shapes optimized for maximum stored light efficiency (solid triangles) and for input Gaussian pulses with the same FWHM (hollow triangles). Also shown are measurements relevant to stored light efficiency: the fraction of the optimized input pulse that escapes the medium before the pulse is stored (open squares). The dashed line combines light storage data at $\tau = 400$ μs and coherence lifetime measurements to predict slow light efficiency (*see text*) in good agreement with measured efficiency. Error bars are from systematic uncertainty in Rb temperature of ~ 2 °C and in the laser frequency of ~ 150 MHz. Error bars on other data sets are of equal magnitude. (b) Sample data for density of approx. 8×10^{11} cm^{-3} showing the retrieved and unstored pulses (dark, solid line), the slow light pulse with optimized shape (dotted line), and the reference pulse (gray solid line).

or high-temperature phenomena adversely affecting slow and stored light. Increased loss during storage and readout at high optical depth agrees with predictions from theoretical simulations when the density dependence of decoherence is included (Fig. 3). The simulations, described fully in earlier work,[18, 21, 22] consist of iterated solutions to the stored light dynamics equations for an ensemble Λ-system. The dashed curve in Fig. 3 uses the measured rates of decoherence during storage and readout taken from Fig. 4 as an input parameter for the spin-wave decay rate, and most closely matches the experimental results.

In Figure 5 we verify that the loss mechanisms for stored light are all self-consistent. A slow light pulse that is not trapped in the medium (the control field is left on) has loss from imperfect EIT contrast and from pulse bandwidth lying outside the region of maximum transmission (after normalization to a reference pulse, this is the "slow-light efficiency"). A stored and retrieved pulse will experience that same loss, and additional loss from two sources: (i) part of the pulse escapes the medium before the pulse is stored (fractional delay less than unity implies significant losses from this mechanism); and (ii) atomic coherence decay during the storage and readout periods. Figure 5a shows the directly measured slow light efficiency η_{slow}, the area ratio of the output pulse to the reference pulse, and an inferred $\eta_{slow,predict}$ from the storage measurement. Using the measured decoherence rate from Fig. 4 and the storage readout areas at $\tau = 400$ μs, we can back out the storage readout at $\tau = 0$; combining this with the area of the not-stored pulse leakage we infer η_{slow} (see Fig. 5b):

$$\eta_{slow,predict} = \eta_{leakage} + \eta \times \exp(400\ \mu s/\tau_{coherence}), \tag{3}$$

where $\eta_{leakage}$ is the leaked pulse area divided by the reference pulse area, and $\tau_{coherence}$ is the atomic coherence lifetime from Fig. 4. The measured and inferred slow light efficiencies match very well, only deviating significantly at the highest atomic density, where the term with $\exp(400\ \mu s/\tau_{coherence})$ becomes very sensitive to the short coherence lifetime measurement, which is more error prone due to the low SNR in the signal transmission.

As indicated from both the storage efficiency and the comparison between slow and stored light, at high Rb densities the effectiveness of the medium decreases. We believe that several mechanisms are contributing to the reduced effectiveness of the rubidium vapor at high densities. First, at higher densities, temperature or density-dependent losses such as rubidium-rubidium spin exchange becomes more significant, contributing to decoherence even during the storage interval (see Fig. 4). Second, in the presence of light at high Rb densities,

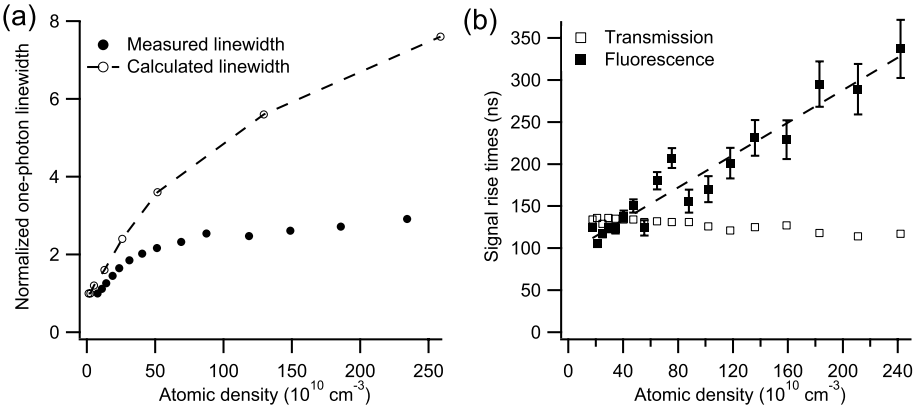

Figure 6. (a) Measured and calculated optical line widths for the signal field when detuned from two-photon resonance as a function of Rb density, consistent with an effectively reduced optical depth at high densities due to radiation trapping. (b) Fluorescence signal rise time increases as the atomic density is increased, whereas transmission signal rise time has minimal density dependence, indicating that absorbed and re-emitted photons are trapped in the medium for a longer time due to the large transverse optical depth. (*See text.*) Error bars are smaller than data points except where shown (derived from uncertainty in Rb temperature).

radiation trapping becomes significant, in which light absorbed and then incoherently radiated by one rubidium atom is reabsorbed by another rubidium atom. This process leads to decoherence and loss of efficiency. In the next sections, we present preliminary investigations of high-density losses.

4. OPTICAL DEPTH AND RADIATION TRAPPING MEASUREMENTS

Direct measurements of large optical depths are difficult due to the large corresponding absorption of the optical field. To characterize the optical depth for comparison with the optimization models described above, we used optical absorption line width as a proxy for the optical depth. The signal field was detuned from two photon resonance by changing the frequency driving the EOM and the signal intensity monitored as the one-photon (laser) detuning was swept through resonance. The line width of the absorption of the signal field serves as a proxy for the optical depth because the log of the measured absorption is proportional to the product of the detuning and the optical depth.

Figure 6a shows a comparison of the measured one-photon linewidth and the expected linewidth from a simple numerical model based on an optically thick sample of three-level Λ-systems. At high densities (and optical depths), the measured linewidth stops growing while the model shows continued line broadening. We attribute this to radiation trapping: photons scattered inside the medium depolarize the rubidium ground state leading to fewer atoms polarized in the signal field channel, leading to both decoherence and absorption of the signal field.

We also directly measured the presence of radiation trapping in our vapor cells, with a simplified apparatus. Light from an extended cavity diode laser was focused through an AOM with a small spot size to allow for rapid rise times in the AOM. This AOM output was turned on and off at a rate of 1 MHz with a rise time of ~ 75 ns. The beam diameter was then expanded to approximately 2 mm and sent into a Rb vapor cell housed inside a small plastic oven, unshielded from stray laboratory magnetic fields, and warmed with resistive heaters to a temperature between 54 and 90 °C. Output light from the cell was measured with two photodetectors: one for transmission and the other for fluorescence mounted to the side of the cell oven where a lens close to the cell focused scattered light onto the detector. When light was turned on via AOM modulation, the rise time of the signal was observed in both detectors.

Evidence for radiation trapping is shown in Fig. 6b. At high atomic densities, the rise time in the fluorescence detection signal increases significantly. The greater the transverse optical depth, the greater the number of

absorption and re-emission cycles that occur before absorbed photons exit the medium, so the rise time seen in fluorescence detection should grow with the transverse optical depth. In Fig. 6b we see rise times up to 350 ns, whereas the lifetime for the excited state of the $5p_{1/2}$ state of Rb is ~ 28 ns, indicating many scattering events for each absorbed photon.

5. NEW VAPOR CELL GEOMETRY

In order to minimize the decoherence resulting from radiation trapping in our vapor cells, we recently developed a cell designed to minimize its effects. A 15 cm long, 1.2 cm diameter cell with N_2 buffer gas was designed to reduce radiation trapping in three ways: (i) the aspect ratio is four times larger than previous cells, allowing fluorescence to escape the cell in the transverse direction with fewer depolarizing interactions with Rb atoms; (ii) the absolute length of the cell is twice that of previous vapor cells allowing the equivalent optical depth to be reached at lower Rb density, minimizing density-dependent effects including spin exchange; (iii) an N_2 buffer gas acts to quench radiation trapping by collisionally de-exciting Rb atoms before the atoms fluoresce, preventing the emission of unpolarized photons that could destroy the coherence of nearby atoms.

Initial results of stored light efficiency in this cell appear promising. For a laser power of $P = 4.5$ mW and a temperature of 58 °C (the same longitudinal optical depth as the density $= 40 \times 10^{10}$ cm^{-3} data in Fig. 3), efficiency of $\eta = 40\%$ was achieved. This is three times greater than the η for $P = 3.8$ mW and twice as great as for $P = 8.8$ mW at the same optical depth. Future measurements will further explore this promising avenue towards high-efficiency light storage in Rb vapor cells.

6. CONCLUSIONS

We reported a preliminary experimental study of slow and stored light at a variety of Rb densities (i.e., optical depths), and as a function of pulse duration, delay and storage time, and control field intensity. Experimental results are in good qualitative agreement with theoretical calculations based on a simplified three-level model at moderate densities; and indicate that radiation trapping is an important limitation at high atomic density. We have developed a new cell geometry which we expect to reduce losses and improve efficiency through reduced radiation trapping and density-dependent decoherence.

We are grateful to A. Glenday for useful discussions. This work was supported by ONR, DARPA, NSF, and the Smithsonian Institution.

REFERENCES

1. C. W. Chou, S. V. Polyakov, A. Kuzmich, and H. J. Kimble, Phys. Rev. Lett. **92**, 213601 (2004).
2. D. N. Matsukevich, and A. Kuzmich, Science **306**, 663 (2004).
3. M. D. Eisaman, L. Childress, A. André, F. Massou, A. S. Zibrov, and M. D. Lukin, Phys. Rev. Lett. **93**, 233602 (2004).
4. D. N. Matsukevich, T. Chanelière, S. D. Jenkins, S.-Y. Lan, T. A. B. Kennedy, and A. Kuzmich, Phys. Rev. Lett. **97**, 013601 (2006).
5. S. Chen, Y.-A. Chen, T. Strassel, Z.-S. Yuan, B. Zhao, J. Schmiedmayer, and J.-W. Pan, Phys. Rev. Lett. **97**, 173004 (2006).
6. C. W. Chou, H. de Riedmatten, D. Felinto, S. V. Polyakov, S. J. van Enk, and H. J. Kimble, Nature **438**, 828 (2005).
7. T. Chanelière, D. N. Matsukevich, S. D. Jenkins, S.-Y. Lan, T. A. B. Kennedy, and A. Kuzmich, Nature **438**, 833 (2005).
8. M. D. Eisaman, A. André, F. Massou, M. Fleischhauer, A. S. Zibrov, and M. D. Lukin, Nature **438**, 837 (2005).
9. T. Chanelière, D. N. Matsukevich, S. D. Jenkins, T. A. B. Kennedy, M. S. Chapman, and A. Kuzmich, Phys. Rev. Lett. **96**, 093604 (2006).
10. L. M. Duan, M. D. Lukin, J. I. Cirac, and P. Zoller, Nature **414**, 413 (2001).

11. D. Felinto, C. W. Chou, J. Laurat, E. W. Schomburg, H. de Riedmatten, and H. J. Kimble, Nature Phys. **2**, 844 (2006).
12. I. Novikova, M. Klein, D. F. Phillips, and R. L. Walsworth, Proc. SPIE-Int. Soc. Opt. Eng. **5735**, 87 (2005).
13. D. Felinto, C. W. Chou, H. de Riedmatten, S. V. Polyakov, and H. J. Kimble, Phys. Rev. A **72**, 053809 (2005).
14. J. Laurat, H. de Riedmatten, D. Felinto, C.-W. Chou, E. W. Schomburg, and H. J. Kimble, Opt. Express **14**, 6912 (2006).
15. J. K. Thompson, J. Simon, H. Loh, and V. Vuletić, Science **313**, 74 (2006).
16. R. S. Tucker, P. S. Ku, and C. J. Chang-Hasnain, J. Lightwave Technol. **23**, 4046 (2005).
17. L. V. Hau, S. E. Harris, Z. Dutton, and C. H. Behroozi, Nature **397**, 594 (1999).
18. M. D. Lukin, Rev. Mod. Phys. **75**, 457 (2003).
19. S. E. Harris and L. V. Hau, Phys. Rev. Lett. **82**, 4611 (1999).
20. M. Fleischhauer and M. D. Lukin, Phys. Rev. A, **65**, 022314 (2002).
21. A. V. Gorshkov, A. Andre, M Fleischhauer, A. S. Sorensen, and M. D. Lukin, Phys. Rev. Lett. **98**, 123601 (2007); A. V. Gorshkov, A. Andre, M. D. Lukin, and A. S. Sorensen, Phys. Rev. A **76**, 033805 (2007).
22. I. Novikova, A. V. Gorshkov, D. F. Phillips, A. S. Srensen, M. D. Lukin, and R. LẆalsworth Phys. Rev. Lett. **98**, 243602 (2007); I. Novikova, A. V. Gorshkov, D. F. Phillips, Y. Xiao, M. Klein, and R. L. Walsworth, Proc. SPIE-Int. Soc. Opt. Eng. **6482**, 64820M-1 (2007).
23. A. F. Molisch and B. P. Oehry, *Radiation Trapping in Atomic Vapors* (Oxford University Press, USA, 1999); A. B. Matsko, I. Novikova, M. O. Scully, and G. R. Welch, Phys. Rev. Lett. **87**, 133601 (2001); A. B. Matsko, I. Novikova, and G. R. Welch, J. Mod. Opt. **49**, 367 (2002).
24. G. Nikoghosyan and G. Grigoryan, Phys. Rev. A **72**, 043814 (2005).